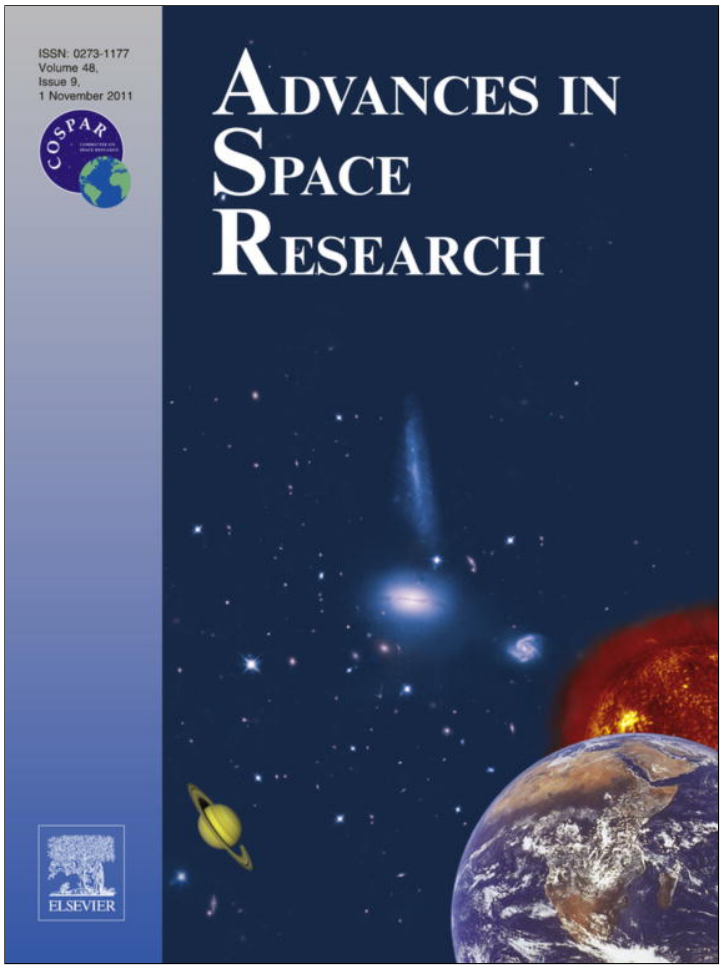

Available online at www.sciencedirect.com
ScienceDirect
Advances in Space Research 48 (2011) 1531–1536
ADVANCES IN SPACE RESEARCH (a COSPAR publication)
www.elsevier.com/locate/asr

Kink-like mode of a double gradient instability in a compressible plasma current sheet

D.B. Korovinskiy [a,*], V.V. Ivanova [b], N.V. Erkaev [c,d], V.S. Semenov [e], I.B. Ivanov [f], H.K. Biernat [a,g], M. Zellinger [a,g]

[a] Space Research Institute, Austrian Academy of Sciences, 8042 Graz, Austria
[b] Orel State Technical University, 302020 Orel, Russia
[c] Institute of Computational Modeling, Russian Academy of Sciences, Siberian Branch, 660036 Krasnoyarsk, Russia
[d] Siberian Federal University, 660041 Krasnoyarsk, Russia
[e] State University of St. Petersburg, 198504 St. Petersburg, Russia
[f] Theoretical Physics Division, Petersburg Nuclear Physics Institute, 188300 Gatchina, Leningrad Region, Russia
[g] Institute of Physics, University of Graz, 8010 Graz, Austria

Received 24 December 2010; received in revised form 20 June 2011; accepted 18 July 2011
Available online 27 July 2011

Abstract

A linear MHD instability of the electric current sheet, characterized by a small normal magnetic field component, varying along the sheet, is investigated. The tangential magnetic field component is modeled by a hyperbolic function, describing Harris-like variations of the field across the sheet. For this problem, which is formulated in a 3D domain, the conventional compressible ideal MHD equations are applied. By assuming Fourier harmonics along the electric current, the linearized 3D equations are reduced to 2D ones. A finite difference numerical scheme is applied to examine the time evolution of small initial perturbations of the plasma parameters. This work is an extended numerical study of the so called "double gradient instability", – a possible candidate for the explanation of flapping oscillations in the magnetotail current sheet, which has been analyzed previously in the framework of a simplified analytical approach for an incompressible plasma. The dispersion curve is obtained for the kink-like mode of the instability. It is shown that this curve demonstrates a quantitative agreement with the previous analytical result. The development of the instability is investigated also for various enhanced values of the normal magnetic field component. It is found that the characteristic values of the growth rate of the instability shows a linear dependence on the square root of the parameter, which scales uniformly the normal component of the magnetic field in the current sheet.

Keywords: Flapping oscillations; Double gradient instability; Current sheet instability

1. Introduction

Flapping oscillations of the magnetotail current sheet have been detected by many spacecraft measurements. In particular, CLUSTER observations in the Earth's magnetotail current sheet indicated the appearance of wave perturbations propagating along the current sheet perpendicular to the magnetic field lines (Zhang et al., 2002; Sergeev et al., 2003, 2004; Runov et al., 2005, 2006; Petrukovich et al., 2006). The CLUSTER observations are in favor of the assumption that the flapping perturbations appear more frequently in the central part of the tail, than near the flanks. In the near-flank tail regions, the flapping waves propagate predominantly from the center to the flanks. These observational results confirm the hypothesis of an internal origin of the flapping motions, due to some nonstationary processes localized deep inside of the magnetotail. The plasma sheet flapping waves are interpreted as quasi-periodic dynamical structures produced by almost

* Corresponding author.
E-mail address: daniil.korovinskiy@gmail.com (D.B. Korovinskiy).

0273-1177/$36.00 © 2011 COSPAR. Published by Elsevier Ltd. All rights reserved.
doi:10.1016/j.asr.2011.07.008

vertical slippage motions of the neighboring magnetic tubes, which allows to identify them as kink-like perturbations. Data analyses allow to estimate the essential parameters of the flapping waves. Spatial amplitudes and wavelengths are found to be of the order of 2–5 Earth's radii (Petrukovich et al., 2006), the typical frequency is estimated to be $\omega_f \sim 0.035$ rad/s (Sergeev et al., 2003), and the generic speed of these waves lies in the range of a few tens (30–70) km $\cdot$ s^{-1} (Runov et al., 2005).

An analytical model of this phenomenon was proposed by Erkaev et al. (2007, 2008, 2009) in the framework of the incompressible MHD approach. For conditions of the Earth's magnetotail current sheet, this model yields estimations of the typical frequency ($\omega_f \sim 0.03$ rad/s) and a group speed (60 km $\cdot$ s^{-1}), demonstrating a good agreement with the CLUSTER observations (Erkaev et al., 2007). In accordance to this model, MHD flapping modes can exist due to a combined effect of gradients of the tangential (B_x) and normal (B_z) magnetic field component along the normal ($\nabla_z B_x$) and tangential ($\nabla_x B_z$) directions with respect to the current sheet. A stable situation for the current sheet is associated with a positive result of the multiplication of the two magnetic gradients, and an unstable (wave growth) condition corresponds to the opposite case, $\nabla_x B_z \nabla_z B_x < 0$. The analytical solution obtained demonstrates two possible modes of the instability, which are kink-like and sausage-like modes. The kink-like mode is characterized by the displacement of the current sheet center, when the perturbation of the tangential component of the velocity, δV_z, is an even function of z. Vice versa, an odd functional behaviour of $\delta V_z(z)$ is relevant to the sausage-like mode, characterized by variations of the thickness of the current layer without displacement of its center (Erkaev et al., 2008). In this paper, we investigate numerically the kink-like mode of the instability and compare our results with analytical predictions of the model of Erkaev et al. (2007–2009), as mentioned above.

2. Qualitative explanation

The geometrical configuration of the problem is illustrated in Fig. 1. The equation of motion in the framework of incompressible ideal MHD for a nonstationary plasma has the following form,

$$\rho\left[\frac{\partial \mathbf{V}}{\partial t} + (\mathbf{V}\cdot\nabla)\mathbf{V}\right] + \nabla P = \frac{\mathbf{1}}{4\pi}(\mathbf{B}\cdot\nabla)\mathbf{B}, \tag{1}$$

where ρ is the plasma density, $\mathbf{V}$ is the plasma bulk velocity, $\mathbf{B}$ is the magnetic field, and P is the total pressure. Let us consider a plasma element of a unit volume, placed at the center of the current layer. In the equilibrium state, the total pressure gradient compensates the magnetic tension,

$$\frac{\partial P}{\partial z} = \frac{1}{4\pi} B_x \frac{\partial B_z}{\partial x}. \tag{2}$$

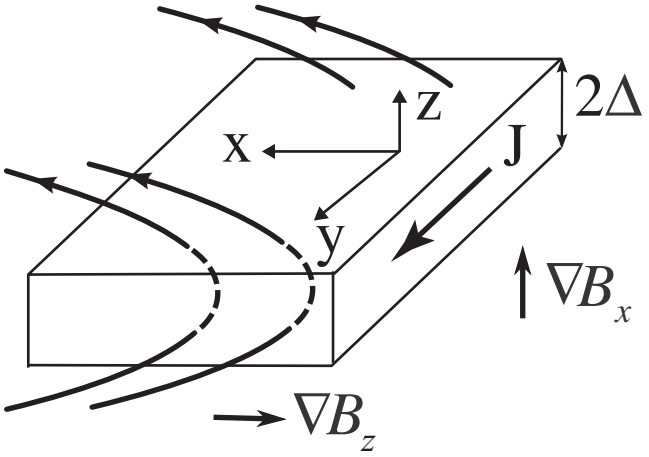

Fig. 1. Geometrical scheme.

A small displacement, δz, of this plasma element along the z-direction yields the restoring force F_z, which is the difference of two forces, caused by the magnetic tension and the total pressure gradient (Erkaev et al., 2009),

$$F_z = -\frac{1}{4\pi}\delta z\left(\frac{\partial B_x}{\partial z}\frac{\partial B_z}{\partial x}\right)_{z=0}, \tag{3}$$

where $B_x(z)$ is determined from a Taylor series expansion. This force accelerates plasma in the z-direction, as shown in Fig. 2. The equation of motion of this plasma element has the form,

$$\frac{\partial^2(\delta z)}{\partial t^2} = -\omega_f^2 \delta z, \tag{4}$$

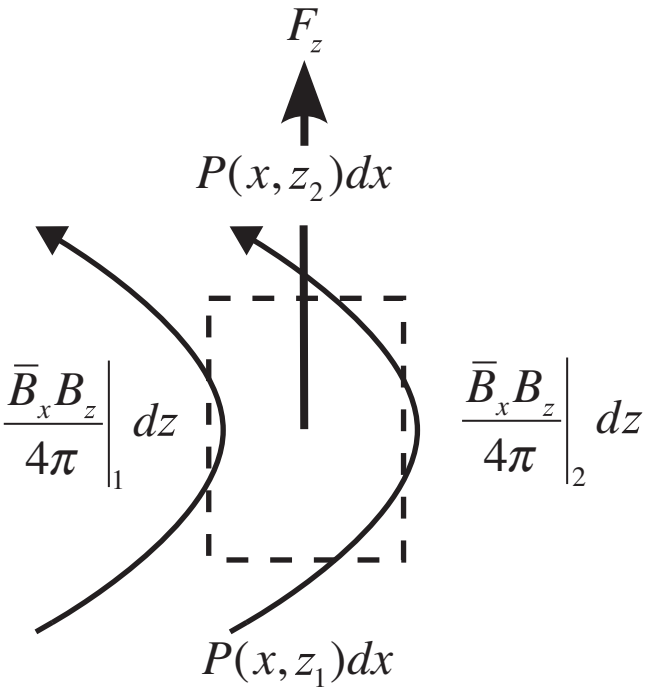

Fig. 2. Small element of the current sheet. After Erkaev et al. (2009).

where

$$\omega_f = \sqrt{\frac{1}{4\pi\rho}\frac{\partial B_x}{\partial z}\frac{\partial B_z}{\partial x}}. \quad (5)$$

In the case of a positive product of the two magnetic gradients, the parameter ω_f is real, and it has the meaning of the characteristic frequency of the flapping wave oscillations. In the opposite case of a negative product of the magnetic gradients, the current sheet is unstable. The flapping perturbations can grow up exponentially without propagation, because ω_f is pure imaginary. These two cases are characterized by a different behaviour of the background total pressure. Specifically, the total pressure has a maximum at the center of the current sheet for an unstable situation, and it has a minimum for stable conditions.

3. Formulation of the problem

We start from the system of the conservative equations of ideal compressible MHD for a non-stationary plasma sheet (Kulikovskii et al., 2001),

$$\frac{\partial \rho}{\partial t} + \nabla\cdot(\rho\mathbf{V}) = 0, \quad (6)$$

$$\frac{\partial(\rho\mathbf{V})}{\partial t} + \nabla\cdot\widehat{\mathbf{\Pi}} = 0, \quad (7)$$

$$\frac{\partial}{\partial t}\left(\frac{\rho V^2}{2} + \rho e + \frac{B^2}{8\pi}\right) + \nabla\cdot\widehat{\mathbf{Q}} = 0, \quad (8)$$

$$\frac{\partial \mathbf{B}}{\partial t} + \nabla\cdot(\mathbf{B}\otimes\mathbf{V} - \mathbf{V}\otimes\mathbf{B}) = 0. \quad (9)$$

Here, $e = p/[\rho(\kappa-1)]$ is the thermal energy in a unit volume, where κ is the polytropic index, and p is the plasma pressure. $\widehat{\mathbf{\Pi}}$ and $\widehat{\mathbf{Q}}$ are the momentum and energy flux densities, respectively,

$$\widehat{\mathbf{\Pi}} = \rho\mathbf{V}\otimes\mathbf{V} + p\widehat{\mathbf{I}} - \frac{1}{4\pi}\left(\mathbf{B}\otimes\mathbf{B} - \frac{B^2}{2}\widehat{\mathbf{I}}\right), \quad (10)$$

$$\widehat{\mathbf{Q}} = \rho\mathbf{V}\left(\frac{V^2}{2} + e + \frac{p}{\rho}\right) + \frac{1}{4\pi}\mathbf{B}\times\mathbf{V}\times\mathbf{B}, \quad (11)$$

where $\widehat{\mathbf{I}}$ is the unitary matrix.

Next, we proceed to normalized quantities, using the set of the constants of normalization, containing the half-width of the current sheet Δ, the magnetic field value at the upper boundary of the sheet $\overline{B}$, the number density at the center of the sheet $\bar{n}$, the proton Alfvén velocity $V_A = \overline{B}/\sqrt{4\pi\bar{n}m_p}$ (where m_p is the proton mass), the pressure $\bar{p} = \overline{B}^2/(4\pi)$, and the time scale $\bar{t} = \Delta/V_A$. Assuming an equilibrium initial state, we apply a perturbation technique to solve equations (6)–(9). Representing all values as the sum of two terms, describing the initial equilibrium state, $\mathbf{U}_0$, and a small perturbation, $\mathbf{U}_1$, we obtain the linearized system of equations for the vector of perturbations,

$$\frac{\partial \mathbf{U}_1}{\partial t} + \frac{\partial \mathbf{F}_x}{\partial x} + \frac{\partial \mathbf{F}_y}{\partial y} + \frac{\partial \mathbf{F}_z}{\partial z} = 0. \quad (12)$$

We search for a solution of this system in the following form, $\mathbf{U}_1(x,y,z) = \delta\mathbf{U}(x,z,t)\exp(iky)$, where k is the wave number. Then, the system of equations for the amplitudes $\delta\mathbf{U}$ may be written as follows,

$$\frac{\partial(\delta\mathbf{U})}{\partial t} + \frac{\partial \mathbf{F}_x}{\partial x} + \frac{\partial \mathbf{F}_z}{\partial z} = \mathbf{S}, \quad (13)$$

where

$$\delta\mathbf{U} = (\delta\rho, \{\rho_0\delta V_i + V_{0i}\delta\rho\}, \{\delta B_i\}, \delta E)_{i=x,y,z}. \quad (14)$$

Here, $\delta E = 0.5V_0^2\delta\rho + \rho_0(\mathbf{V}_0\cdot\delta\mathbf{V}) + (\mathbf{B}_0\cdot\delta\mathbf{B}) + \delta p/(\kappa-1)$. The expressions for the flux densities $\mathbf{F}_x$ and $\mathbf{F}_z$ and for the source function $\mathbf{S}$ are given in Appendix A.

4. Numeric scheme and results

We proceed to get a solution of the system (13), using a Lax–Friedrichs finite difference method (Chu, 1978), which is forward in time and centered in space an one-step first order scheme. The initial background state is chosen to be a Harris-like configuration with a linear normal component of the magnetic field. We use the GSM coordinate system, rotated by 180° around the z axis, with its center shifted to the magnetotail, so that the initial configuration is fixed as follows,

$$B_{0x} = -\tanh(z), \quad \mathbf{V}_0 = 0,$$
$$B_{0z} = a + bx, \quad B_{0y} = 0.$$

These background conditions are similar to those used by Erkaev et al. (2007) in their analytical approach. At any cross-section of the sheet, the gas pressure, p^*, is determined from the static equation $\nabla_z p^* = -j_{0y}B_{0x}$, wherefrom $p^* = p_0 - \tanh^2(z)/2 - b\ln[\cosh(z)]$. The pressure distribution along x-direction is found from the equation $\nabla_x p = j_{0y}B_{0z}$, from which follows that $p = p^* + \int_0^x j_{0y}B_{0z}dx'$, which yields,

$$p = p_0 - \left(ax + \frac{bx^2}{2}\right)\left(b + \frac{1}{\cosh^2(z)}\right) - \frac{\tanh^2(z)}{2} - b \times \ln[\cosh(z)]. \quad (15)$$

The constant values are $\kappa = 5/3$, $p_0 = 5$, $\rho_0 = 1$, $a = 0.1$, and $b = 0.01$. The initial distribution of the total pressure is shown in Fig. 3. The total pressure has a maximum at the center of the sheet, and the product of the gradients of the magnetic field components is negative, so that the physical conditions for the growth of the instability, discussed in Section 2, are fulfilled.

The boundary conditions used for the upper and lower boundaries, $\bar{z} = \{z_{max}, z_{min}\}$, are,

$$\delta\mathbf{U}(x,\bar{z}) = 0. \quad (16)$$

This choice assumes the computational domain to be wide enough, so that perturbations fade out far away from the current sheet, in accordance to the solution for the eigenfunctions, obtained by Erkaev et al. (2009). These eigenfunctions do not depend on the x-coordinate value, as well as our

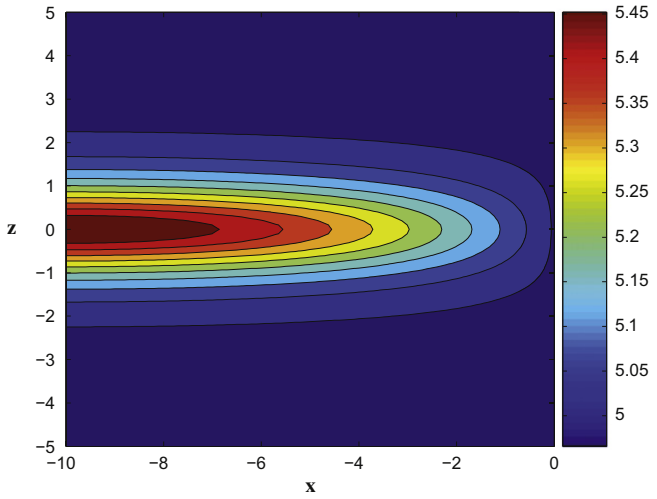

Fig. 3. Initial distribution of the total pressure in normalized units.

initial perturbation $\delta V_z = \exp(-z^2)$. Therefore, the boundary conditions at the right and left boundaries, $\bar{x} = \{x_{max}, x_{min}\}$, are chosen as follows,

$$\frac{\partial(\delta \mathbf{U})}{\partial x}(\bar{x}, z) = 0. \tag{17}$$

We now solve system (13) for several fixed values of the wave number k to obtain the dispersion curve $\omega(k)$. Since ω is a pure imaginary quantity in our situation, its imaginary part is the growth rate of the instability. We denote it by γ, $\gamma \equiv \mathrm{Im}[\omega]$. In Fig. 4, the typical picture of the development of the instability for $k = 5$ is presented.

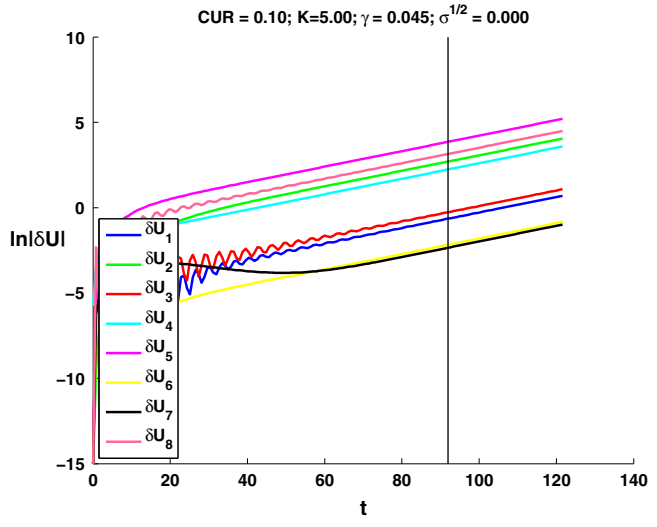

Fig. 4. Time evolution of the perturbation amplitudes. The wave number is $k = 5$, the growth rate is $\mathrm{Im}[\omega] = 0.045$, the standard deviation is $\sigma < 10^{-3}$. The black vertical line marks the left boundary of the interval of the calculation of ω and σ. The amplitudes $\delta\mathbf{U} = (\delta\rho, \{\delta V_k\}, \{\delta B_k\}, \delta E)_{k=\{x,y,z\}}$ are calculated in the fixed point $x = -7.4$, $z = -2.4$. Note that the pink curve demonstrates the evolution of the absolute value of the energy perturbation in the single point. The total energy perturbation fulfills $\int \delta E dx dz = 0$.

The numeric viscosity of the scheme leads to an artificial reduction of the growth rate. To estimate the genuine value of γ we use the Richardson-like extrapolation (Richardson, 1911), which assumes the scheme damping to be proportional to the mesh step, so that $\gamma^*(k) = \gamma(k) - A(k)h$, where γ^* is the computed value of γ, quantity h is the mesh step, and $A(k)$ is some coefficient which is independent of h. Then, the extrapolating expression takes the form,

$$\gamma = 2\gamma^*_{h/2} - \gamma^*_h, \tag{18}$$

where γ^*_h and $\gamma^*_{h/2}$ are the values of the growth rate obtained by using the two computational grids with steps h and $h/2$, respectively. Note that γ obtained by formula (18) is a second order approximation (of the genuine quantity), while values γ^*_h and $\gamma^*_{h/2}$ are first order ones.

So, we perform our calculations in the rectangular box $[x \times z] = [(-10 \ldots 0) \times (-5 \ldots 5)]$, at the two uniform grids with sizes $[101 \times 401]$ and $[201 \times 801]$. The typical Courant number $C = 0.1$ is used in both runs. In Fig. 5, the dispersion curves $\gamma^*_h(k), \gamma^*_{h/2}(k)$ and $\gamma(k)$ are plotted, as well as the analytical prediction as given by Erkaev et al. (2007), which has the form,

$$\gamma(k) = \mathrm{Im}[\omega_f]\sqrt{\frac{k}{k+1}}, \tag{19}$$

where ω_f is described by formula (5). Thus, the numeric value $\mathrm{Im}[\omega_f] = 0.08$ turns out to be 20% less than the analytical one (0.1), yielded by the definition (5).

One can see that under the definition (15) of the plasma pressure, the equilibrium condition $\nabla p = \nabla \times \mathbf{B} \times \mathbf{B}$ is satisfied along the x direction, but not across the sheet. This means that the non-zero force acts in the z direction producing the perturbation, which grows in time linearly. However, after a while, this perturbation must become negligible to be compared to the exponentially growing

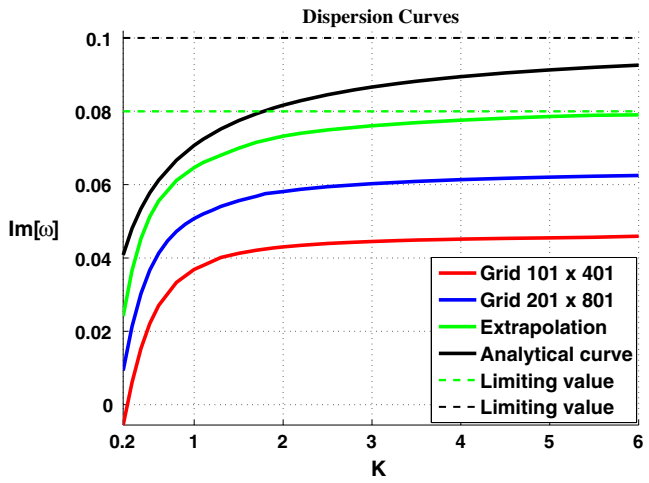

Fig. 5. Dispersion curves for the kink instability, calculated at the grids 101×401 (red) and 201×801 (blue). The dispersion curve, obtained by using the Richardson-like extrapolation (green), and the analytical prediction (black), as obtained by Erkaev et al. (2007). The dotted lines mark the corresponding limiting values $\mathrm{Im}[\omega_f]$.

double-gradient instability. Therefore, the deviation of the plasma pressure fixed in the form of (15) from the equilibrium distribution (which is unknown) corresponding to the given configuration of the magnetic field, impacts the obtained results in a minor way only. To confirm this speculation, we performed calculations with the pressure distribution, satisfying the equilibrium condition in the z direction,

$$\tilde{p} = p_0 - \left(ax + \frac{bx^2}{2}\right)(b+1) - -\frac{\tanh^2(z)}{2} - b\ln[\cosh(z)], \quad (20)$$

and calculations with the plasma pressure depending on the magnetic potential A only (that is uniform along the field lines),

$$\tilde{\tilde{p}} = p_0 - (b+1)A, \quad (21)$$

$$A = ax + \frac{bx^2}{2} + \ln[\cosh(z)], \quad (22)$$

where $(B_x, B_z) = \nabla A \times \mathbf{e}_y$, and $\mathbf{e}_y$ is the unit vector in the direction of the y axis. The results of the runs with these three distributions of the pressure are compared in Fig. 6. The difference between growth rates of the instability amounts 2–5%, decreasing for the larger wave numbers.

The development of the instability is also investigated for the range of enhanced values of the normal magnetic field component, for which the analytical model is not applicable. In Fig. 7, we present the dependence of the quantity $\mathrm{Im}[\omega_f]$ on the value of the normal component of the magnetic field, B_z. The limiting value of the growth rate, $\mathrm{Im}[\omega_f]$, is calculated for $B_z = \alpha(0.1 + 0.01x)$, where $\alpha = \{1, 2, 4, 6, 8, 10\}$. Quantity $\mathrm{Im}[\omega_f]$ shows a linear dependence on the square root of α.

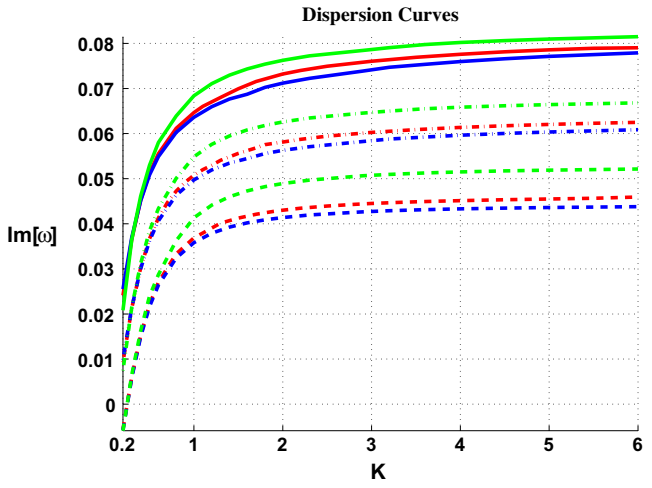

Fig. 6. Dispersion curves for three distributions of the plasma pressure. Red curves are obtained with the expression (15) for p, blue – with the expression (20) for $\tilde{p}$, and green – with the expression (21) for $\tilde{\tilde{p}}$. Dashed lines mark the curves calculated at the grid 101 × 401, dashed-doted lines – at the grid 201 × 801, and solid lines show Richardson extrapolations.

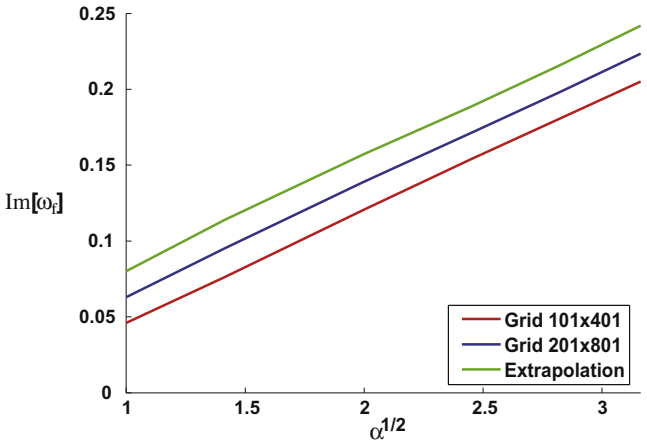

Fig. 7. Limiting growth rate $\mathrm{Im}[\omega_f]$ as a function of parameter α, scaling the B_z value, $B_z = \alpha(0.1 + 0.01x)$. The calculations are performed at the grids 101 × 401 (red), and 201 × 801 (blue). The curve, obtained by using the Richardson-like extrapolation, is plotted by green color.

5. Conclusions

The dispersion curve is calculated numerically for the kink-like mode of the magnetic double gradient instability. The numeric discrepancy in the typical growth rate value (short-wavelength limit) between the calculations and analytical prediction amounts 20%. One of the expectable reasons of this disagreement could be the compressibility of the plasma, which has been neglected in the analytical model. Though, few runs with enhanced values of the polytropic index κ disprove this assumption as well as calculations for the case of an incompressible plasma. The dispersion curves obtained for $\kappa = (5/3)\beta$, where $\beta = \{1, 10^2, 10^4, 10^6\}$, and for $\delta\rho = 0$ are found to be absolutely identical to each other, demonstrating the independence of the growth rate on the compressibility.

There is another difference of the mathematical treatments applied in numeric and analytical solutions. Namely, the analytical model is developed in the frame of quasi-1D MHD, while the numerical solution is obtained for a 2D model. This means that some small terms of the linearized MHD system, which have been neglected in the analytical solution (Erkaev et al., 2009), may be responsible for the observed disagreement between the two solutions.

The development of the instability is investigated also for the range of enhanced values of the normal magnetic field component. It is found that typical values of the growth rate demonstrate a linear dependence on the square root of the parameter, which scales uniformly the B_z value in the current sheet. This result confirms partially the analytical prediction (5), claiming the typical frequency (growth rate) to be proportional to the square root of the gradient of the normal component of the magnetic field.

Altogether, the numerical investigation of the double-gradient mechanism confirms to a high extent the analytical prediction, claiming that the kink-like instability develops in a current sheet with a reverse gradient of the normal

component of the magnetic field, $\nabla_x B_z < 0$. Note that configurations of this kind necessarily occur in the terrestrial magnetotail, preceding the formation of magnetic reconnection events. As the instability proceeds, the current sheet exhibits growing "finger" structures, which are similar to the classical Rayleigh-Taylor instability.

Acknowledgments

This work is supported by the Austrian Science Fund under project I193-N16, by RFBR Grant No. 09-05-91000-ANF-a, by SPSU grant No. 11.38.47.2011, and by the European Union Seventh Framework Programme [FP7/2007-2013] under grant agreement No. 269198 – Geoplasmas (Marie Curie International Research Staff Exchange Scheme). V.S. Semenov thanks also ISSI for hospitality and financial support.

Appendix A. Flux densities and source function

The flux densities $\mathbf{F}_x$, $\mathbf{F}_z$, and the source function $\mathbf{S}$ in the Eq. (13) are given in the following equalities,

$$
\begin{aligned}
&F_{x1} = V_{0x}\delta\rho + \rho_0\delta V_x,\\
&F_{x2} = V_{0x}^2\delta\rho + 2\rho_0 V_{0x}\delta V_x - 2B_{0x}\delta B_x + \delta p + (\mathbf{B}_0\cdot\delta\mathbf{B}),\\
&F_{x3} = \rho_0(V_{0x}\delta V_y + V_{0y}\delta V_x) + V_{0x}V_{0y}\delta\rho - B_{0x}\delta B_y - B_{0y}\delta B_x,\\
&F_{x4} = \rho_0(V_{0x}\delta V_z + V_{0z}\delta V_x) + V_{0x}V_{0z}\delta\rho - B_{0x}\delta B_z - B_{0z}\delta B_x,\\
&F_{x5} = 0,\quad F_{x6} = V_{0x}\delta B_y + B_{0y}\delta V_x - B_{0x}\delta V_y - V_{0y}\delta B_x,\\
&F_{x7} = V_{0x}\delta B_z + B_{0z}\delta V_x - B_{0x}\delta V_z - V_{0z}\delta B_x,\\
&F_{x8} = \delta(\widehat{E}V_x) - B_{0x}[(\mathbf{B}_0\cdot\delta\mathbf{V}) + (\mathbf{V}_0\cdot\delta\mathbf{B})] - B_0V_0\delta V_x,\\
&F_{z1} = V_{0z}\delta\rho + \rho_0\delta V_z,\\
&F_{z2} = \rho_0(V_{0x}\delta V_z + V_{0z}\delta V_x) + V_{0x}V_{0z}\delta\rho - B_{0z}\delta B_x - B_{0x}\delta B_z,\\
&F_{z3} = \rho_0(V_{0y}\delta V_z + V_{0z}\delta V_y) + V_{0y}V_{0z}\delta\rho - B_{0z}\delta B_y - B_{0y}\delta B_z,\\
&F_{z4} = V_{0z}^2\delta\rho + 2\rho_0 V_{0z}\delta V_z - 2B_{0z}\delta B_z + \delta p + (\mathbf{B}_0\cdot\delta\mathbf{B}),\\
&F_{z5} = V_{0z}\delta B_x + B_{0x}\delta V_z - B_{0z}\delta V_x - V_{0x}\delta B_z,\\
&F_{z6} = V_{0z}\delta B_y + B_{0y}\delta V_z - B_{0z}\delta V_y - V_{0y}\delta B_z,\\
&F_{z7} = 0,\quad F_{z8} = \delta(\widehat{E}V_z) - B_{0z}[(\mathbf{B}_0\cdot\delta\mathbf{V}) + (\mathbf{V}_0\cdot\delta\mathbf{B})] - B_0V_0\delta V_z,\\
&S_1 = -ik[V_{0y}\delta\rho + \rho_0\delta V_y],\quad S_2 = -ik[\rho_0(V_{0x}\delta V_y + V_{0y}\delta V_x)\\
&\quad + V_{0x}V_{0y}\delta\rho - B_{0x}\delta B_y - B_{0y}\delta B_x],\quad S_3 = -ik[V_{0y}^2\delta\rho\\
&\quad + 2\rho_0 V_{0y}\delta V_y - 2B_{0y}\delta B_y + \delta p + (\mathbf{B}_0\cdot\delta\mathbf{B})],\\
&S_4 = -ik[\rho_0(V_{0z}\delta V_y + V_{0y}\delta V_z) + V_{0y}V_{0z}\delta\rho - B_{0y}\delta B_z - B_{0z}\delta B_y],\\
&S_5 = -ik[V_{0y}\delta B_x + B_{0x}\delta V_y - B_{0y}\delta V_x - V_{0x}\delta B_y],\\
&S_6 = 0,\quad S_7 = -ik[V_{0y}\delta B_z + B_{0z}\delta V_y - B_{0y}\delta V_z - V_{0z}\delta B_y],\\
&S_8 = -ik[\delta(\widehat{E}V_y) - B_{0y}[(\mathbf{B}_0\cdot\delta\mathbf{V}) + (\mathbf{V}_0\cdot\delta\mathbf{B})] - B_0V_0\delta V_y],
\end{aligned}
$$

where

$$
\begin{aligned}
&\delta(\widehat{E}V_j) = (\widehat{E}_0\delta V_j + V_{0j}\delta\widehat{E})|_{j=\{x,y,z\}},\\
&\widehat{E}_0 = 0.5\rho_0V_0^2 + B_0^2 + p_0\kappa/(\kappa-1),\\
&\delta\widehat{E} = \delta E + \delta p + (\mathbf{B}_0\cdot\delta\mathbf{B}),\\
&\delta p = (\kappa-1)\big(\delta E - 0.5V_0^2\delta\rho - \rho_0(\mathbf{V}_0\cdot\delta\mathbf{V}) - (\mathbf{B}_0\cdot\delta\mathbf{B})\big).
\end{aligned}
$$

References

Chu, C.K. Numerical Methods in Fluid Mechanics. Advances in Applied Mechanics, Vol. 18. Academic Press, New York, ISBN 978-0-120-020188, 1978.

Erkaev, N.V., Semenov, V.S., Biernat, H.K. Magnetic double-gradient instability and flapping waves in a current sheet. Phys. Rev. Lett. 99, 235003, doi:10.1103/PhysRevLett.99.235003, 2007.

Erkaev, N.V., Semenov, V.S., Biernat, H.K. Magnetic double-gradient mechanism for flapping oscillations of a current sheet. Geophys. Res. Lett. 35, L02111, doi:10.1029/2007GL032277, 2008.

Erkaev, N.V., Semenov, V.S., Kubyshkin, I.V., Kubyshkina, M.V., Biernat, H.K. MHD aspect of current sheet oscillations related to magnetic field gradient. Ann. Geophys. 27, 417–425, 2009.

Kulikovskii, A.G., Pogorelov, N.V., Semenov, A.Yu. Mathematical Aspects of Numerical Solution of Hyperbolic Systems. Chapman&Hall/CRC, 2001.

Petrukovich, A.A., Zhang, T.I., Baumjohann, W., Nakamura, R., Runov, A., Balogh, A., Carr, C. Oscillatory magnetic flux tube slippage in the plasma sheet. Ann. Geophys. 24, 1695–1704, 2006.

Richardson, L.F. The approximate arithmetical solution by finite differences of physical problems including differential equations, with an application to the stresses in a masonry dam. Phil. Trans. Royal Soc. Lond. A 210, 307–357, doi:10.1098/rsta.1911.0009, 1911.

Runov, A., Sergeev, V.A., Baumjohann, W., Nakamura, R., Apatenkov, S., Asano, Y., Volwerk, M., Vörös, Z., Zhang, T.L., Petrukovich, A., Balogh, A., Sauvaud, J.-A., Klecker, B., Rème, H. Electric current and magnetic field geometry in flapping magnetotail current sheets. Ann. Geophys. 23, 1391–1403, 2005.

Runov, A., Sergeev, V.A., Nakamura, R., Baumjohann, W., Apatenkov, S., Asano, Y., Takada, T., Volwerk, M., Vörös, Z., Zhang, T.L., Sauvaud, J.-A., Rème, H., Baloghand, A. Local structure of the magnetotail current sheet: 2001 cluster observations. Ann. Geophys. 24, 247–262, 2006.

Sergeev, V., Runov, A., Baumjohann, W., Nakamura, R., Zhang, T.L., Volwerk, M., Balogh, A., Rème, H., Sauvaud, J.-A., Andre, M., Klecker, B. Current sheet flapping motion and structure observed by Cluster. Geophys. Res. Lett. 30, 1327, doi:10.1029/ 2002GL016500, 2003.

Sergeev, V., Runov, A., Baumjohann, W., Nakamura, R., Zhang, T.L., Balogh, A., Louarnd, P., Sauvaud, J.-A., Rème, H. Orientation and propagation of current sheet oscillations. Geophys. Res. Lett. 30, L05807, doi:10.1029/2003GL019346, 2004.

Zhang, T.L., Baumjohann, W., Nakamura, R., Balogh, A., Glassmeier, K.-H. A wavy twisted neutral sheet observed by CLUSTER. Geophys. Res. Lett. 29, 1899, doi:10.1029/2002GL015544, 2002.